Physica E 143 (2022) 115391

Contents lists available at ScienceDirect

Physica E: Low-dimensional Systems and Nanostructures

journal homepage: www.elsevier.com/locate/physe

Scanning tunneling microscopy study of the antiferromagnetic topological insulator $MnBi_2Se_4$

Robert C. Walko [a], Tiancong Zhu [a], Alexander J. Bishop [a], Roland K. Kawakami [a], Jay A. Gupta [a,*]

[a] Department of Physics, The Ohio State University, Columbus, OH, 43210, USA

A B S T R A C T

Topological insulators with intrinsic magnetic ordering such as $MnBi_2Se_4$ have been predicted to host many exotic topological phenomena including dissipationless edge states and magnetoelectric effects. Here we use scanning tunneling microscopy to study the surface of $MnBi_2Se_4$ epitaxial thin films. Large scale topographic images show steps between van der Waals layers and screw dislocations. While we find the Se-termination predominant on the surface, areas attributed to Bi-termination are found at the edges of small islands in as-grown films, or in larger areas upon removal of surface capping. We compare these terminations through an analysis of step heights, atomic resolution images and tunneling spectroscopy. Tunneling spectra on the Se-termination reveals semiconducting behavior, with an apparent bandgap of >0.18 eV that depends on the tip height. In contrast, tunneling spectra of the Bi-termination appears gapless, which could be an indication of dangling bond states on the surface. In both cases, a hexagonal 3.9 Å lattice is observed that is consistent with the expected crystal structure.

1. Introduction

Introducing magnetism to topological insulators (TIs) can lead to the opening of a gap in the topological surface states, and has been predicted to lead to a variety of interesting phenomena such as magnetoelectric effects, Weyl semimetal phases, and the quantum anomalous Hall effect [1–4]. Initial attempts to create magnetic TIs focused on doping traditional TIs with magnetic impurities such as V, Cr, Fe, and Mn [5–8]. Another approach toward this end with the potential to reduce disorder from random doping, is to realize intrinsically magnetic TIs, which are stoichiometric crystals with magnetic ordering. For example, members of the MnX_2Y_4 (X = Bi or Sb, Y = Te, Se, or S) family of materials were predicted to exhibit layer-wise A-type antiferromagnetic ordering, while retaining TI properties [3,4,9,10]. These materials are related to Bi_2Se_3/Bi_2Te_3 and share a similar van der Waals (VdW) layered structure, with a Mn layer in the middle of a septuple layer (SL) repeat unit providing the magnetic moments. Promising experimental confirmation of predictions in $MnBi_2Te_4$ [11–14] has motivated subsequent studies in this family, including our work in $MnBi_2Se_4$ [15], and recent studies of $MnSb_2Te_4$ [16]. Together, this family of compounds offers the potential for independent tuning of magnetism and topological properties through doping, alloying and heterostructures.

Unlike bulk band structure, topological surface states can have an additional susceptibility to the real-space structure of the physical specimen. Therefore, they can be sensitive to features including variations in the number of layers (e.g. even/odd effects), step edges, point defects, adsorbates, surface dipoles, screw dislocations, and surface terminations, all of which can be studied in a surface science context on epitaxial thin films. This motivates our report here of the first STM study of $MnBi_2Se_4$ thin films, grown using molecular beam epitaxy. Topographic images reveal atomically flat areas as well as triangular shaped peninsulas with septuple layer high step edges. While we find the Se-termination predominant on the surface, areas attributed to Bi-termination are found at the edges of small islands in as-grown films, or in larger areas upon removal of surface capping. We compare these terminations through an analysis of step heights, atomic resolution images and tunneling spectroscopy. Tunneling spectra on the Se-termination reveals semiconducting behavior, with an apparent bandgap that increases significantly with the tip height. Two classes of defects are studied in the Se-terminated surface, including one we attribute to a 2nd layer Mn_{Bi} point defect, and one which images with more diffuse contrast that we attribute to a deeper subsurface charged defect. In contrast, tunneling spectra of the Bi-termination appears gapless, which could be an indication of dangling bond states on the surface. In both cases, a hexagonal 3.9 Å lattice is observed that is consistent with the $MnBi_2Se_4$ crystal structure.

2. Experimental methods

STM measurements were performed under ultra-high vacuum (UHV) at 5 K in a Createc LT-STM with a base pressure of 1×10^{-10} mbar. An electrochemically etched Cr tip was used for all data presented here. The

* Corresponding author.
E-mail address: gupta.208@osu.edu (J.A. Gupta).

https://doi.org/10.1016/j.physe.2022.115391
Received 22 June 2022; Accepted 23 June 2022
Available online 25 June 2022
1386-9477/© 2022 Elsevier B.V. All rights reserved.

tip was prepared for imaging by Ar^+ ion sputtering and field emission on a Cr (001) single crystal sample. Scanning tunneling spectroscopy (STS) measurements were performed using lock-in detection of the differential conductance, dI/dV, by adding an AC bias modulation of 15–50 mV_{rms} at 1036 Hz and with the feedback loop turned off to keep the tip-sample separation constant as the bias voltage is swept. We also acquired simultaneous topographic and dI/dV maps at fixed voltage by using the same lock-in technique with the feedback loop on. Analysis of STM images was performed using SPIP analysis software.

Three samples were studied in this work, all of which were grown by molecular beam epitaxy (MBE) to a thickness of 20 SLs using the methods previously reported [15]. Sample A was grown on a sapphire substrate and then capped with ~10 nm of amorphous Se to protect the surface during *ex situ* characterization by magnetometry and x-ray diffraction [15]. The Se cap was removed prior to STM imaging by returning the sample to UHV and annealing at ~150 °C. To probe the influences of substrate and capping, we also studied Sample B (GaAs (111) substrate, no Se cap) and Sample C (sapphire, no Se cap) prepared under otherwise identical growth conditions. All samples were transferred from the growth chamber to the STM chamber using a Ferrovac UHV suitcase, and all samples were imaged without any additional surface preparation. Discussed further below and in the supplement, all three samples exhibited similar surface quality (c.f, Fig. S1).

3. Results and discussion

3.1. Layered structure of $MnBi_2Se_4$

$MnBi_2Se_4$ is a layered material with the space group $R\bar{3}m$. It is formed of SLs separated by a van der Waals (vdW) gap, shown in Fig. 1a, with a stacking order within each SL of Se–Bi–Se–Mn–Se–Bi–Se. Each layer within an SL is comprised of a triangular lattice of atoms. Density functional theory (DFT) calculations have predicted an in-plane lattice constant of between 3.93 and 4.22 Å and a distance between SLs of 12.26–13.05 Å [4,10,15,17,18]. The surface of layered materials can terminate on different layers, but due to the weak vdW bonding between SLs and the Se-rich growth conditions, we expect the top Se layer to be the energetically preferred surface termination, similar to what has been observed in other vdW materials like Bi_2Se_3 and Bi_2Te_3[19].

In Fig. 1b we show a large scale topographic STM image of the surface to investigate the overall film morphology. Large, atomically flat areas that appear smooth are seen in the topographic imaging at this scale, as well as peninsulas that lead to height variations across the image of roughly ±1 SL. In the atomically flat areas, we note some sloping across the surface due to the presence of screw dislocations (SDs), examples of which are highlighted with red circles. Upon close inspection it is clear that most of the surface is smoothly connected due to the SDs which implies that those areas should all be the same surface termination. This surface termination is the clear majority across all areas imaged on our sample and so *a priori* we assign it as the Se termination. This assignment will be discussed further below and is similar to prior STM studies of the Te termination of $MnBi_2Te_4$ [20–24].

Fig. 1cis an enlarged version of the boxed area in Fig. 1b with the three lines representing the locations of height profiles plotted in Fig. 1d. The blue profile, which was taken along the upper right edge of the peninsula, shows a step height of approximately 12.2 Å, close to the range of heights predicted for an SL step. There is significant variation in the step heights measured for this peninsula because it forms from an SD (the red circle Fig. 1b just below the bottom right edge of the box). This is demonstrated by the green profile which was taken closer to the SD and has a step height of ~6 Å. In general, the measured step height goes to zero for profiles taken close to the SD origin. However, the fact the step height approaches the SL height away from the SD shows that peninsulas that originate from SDs still form full SLs. At the top of this peninsula, there is a small triangular-shaped region which we attribute to a distinct surface termination. The red profile across the top of the peninsula shows an intermediate partial step down by 1.6 Å relative to the peninsula surface, which is close to that expected for the next Bi layer based on the crystal structure (Fig. 1a) [17]. We will discuss this assignment in more detail below.

3.1.1. Se-terminated surface

Fig. 2 shows atomic resolution images and spectroscopy of the predominant Se-terminated surface. The topographic image shows a random background distribution of bright contrast on ~5 nm length scales that we attribute to charged subsurface defects, similar to prior STM studies of other semiconductor surfaces [25–27]. At the atomic

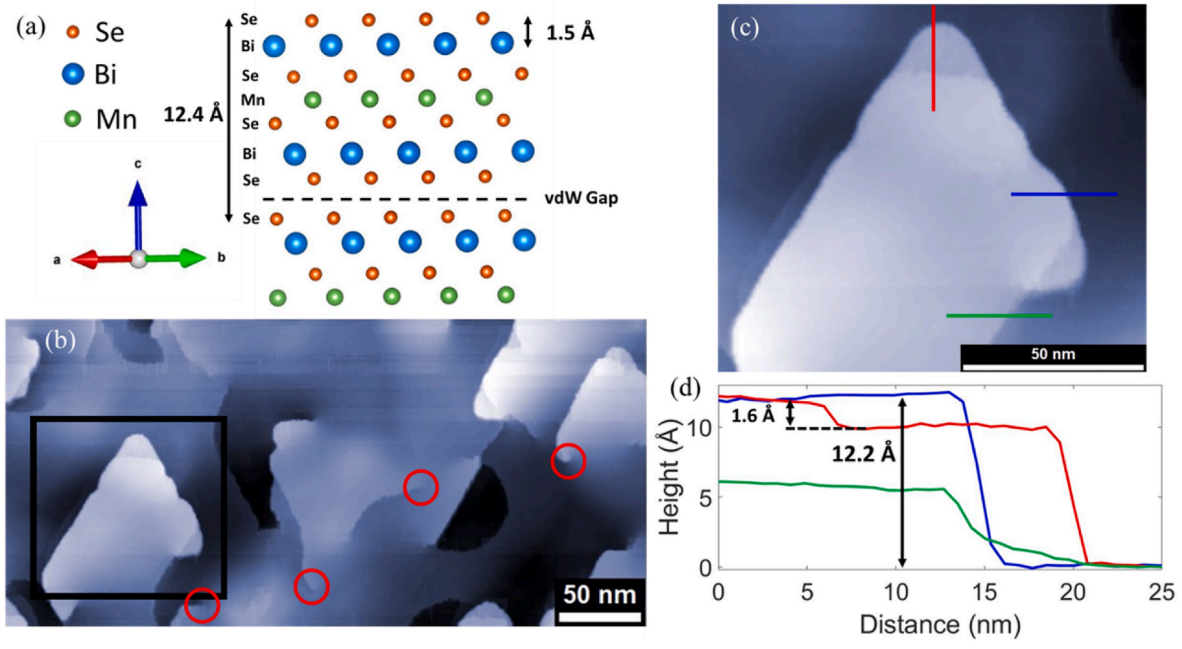

Fig. 1. $MnBi_2Se_4$ film morphology. (a) Side view of the crystal structure. (b) Topographic STM image (−2.0 V, 0.2 nA) of the surface with red circles highlighting some of the screw dislocations. (c) zoom in of the boxed area in (b). (d) Height profiles corresponding to the red, blue, and green lines in (c). Data taken on Sample A.

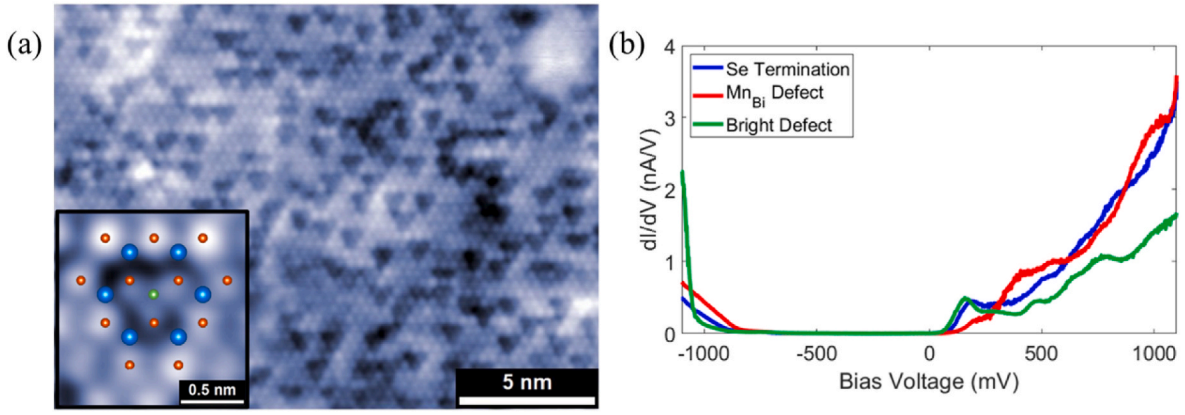

Fig. 2. STM imaging and spectroscopy of the Se termination. (a) Atomic resolution image of the Se termination (−1.0 V, 0.54 nA). The inset shows a Mn_{Bi} defect with an overlay indicating the atomic structure (colors as in Fig. 1a). (b) Tunneling spectra taken on the bare Se termination, a Mn_{Bi} defect, and the unidentified bright subsurface defect (tip height set at −1.1 V and 0.53 nA, $V_{AC} = 50\ mV_{rms}$). The specific location that each spectrum was taken at is shown in Fig. S2. Data taken on Sample A.

scale, a triangular lattice of bright spots is observed that is attributed to the surface Se atoms, with a spacing of 3.9 ± 0.1 Å, consistent with DFT calculations [4,10,15,17,18]. A number of point defects that image with dark, three-fold symmetric contrast are also apparent. We attribute these to Mn_{Bi} antisite defects, which consist of a Mn atom substituted in the location of a Bi atom, as depicted by the overlay in the inset of Fig. 2a. Since we are imaging the Se termination, the defect lies in the Bi layer directly below the surface, and the Mn atom is bonded with three Se atoms in the top layer. This explains the continuity of the Se triangular lattice over the defects in Fig. 2a, as the Se atoms bonded to Mn_{Bi} should be imaged with distinct contrast from Se bonded to Bi. Recent STM studies of $MnBi_2Te_4$ have also observed antisite defects with similar characteristics [21–23]. From larger scale atomic resolution images, we estimate a surface Mn_{Bi} defect density of ~5 × 10 [13] cm^{-2} which corresponds to about ~10% of Bi sites being substituted for Mn.

Scanning tunneling spectroscopy (STS) was performed to probe the local density of states (LDOS) of the Se termination and the characteristic Mn_{Bi} point defect and subsurface bright defect regions (Fig. 2b). Tunneling spectra taken with the tip positioned on a Se atom shows semiconducting behavior, with an apparent band gap of ~700 meV and a Fermi level near the conduction band edge. On the Mn_{Bi} defect, STS shows a slight enhancement in the LDOS of the occupied states at negative voltage, as well as a suppression of the unoccupied states at around +100 mV, which is similar to spectra taken on Mn_{Bi} antisite defects in $MnBi_2Te_4$ [23]. The apparent band gap appears unaffected by the presence of the antisite defect, and the defect does not contribute significant in-gap LDOS. Finally, spectra taken on the bright subsurface defects show a sharp increase in the LDOS in occupied states relative to the other two spectra, but otherwise a qualitatively similar absence of in-gap states and unoccupied state LDOS.

The apparent bandgap in Fig. 2b is significantly larger than the bandgap of <200 meV we previously measured by ARPES [15], and inferred from thermally-activated transport measurements of bulk crystals [28]. To better understand this difference we performed STS measurements with varying tip-sample separation. While the absolute tip height is only approximately known (~7–10 Å), we can precisely vary the relative tip height by small offsets of the z-piezo voltage before the bias is swept. Data were then assembled into the color plot in Fig. 3a, with a log scale to emphasize the changes with tip height. We find that the size of the apparent band gap (dark blue region in the color map) dramatically decreases as the tip gets closer to the sample, going from a value of ≥1700 meV at the largest tip sample separation, to about 340 meV when the tip is moved 2 Å closer. Fig. 3b shows that this trend continues down to the closest approach (3.5 Å) where we could still maintain stable tunneling conditions. The apparent bandgap in these data is ~180 meV, which is in good agreement with previous reports

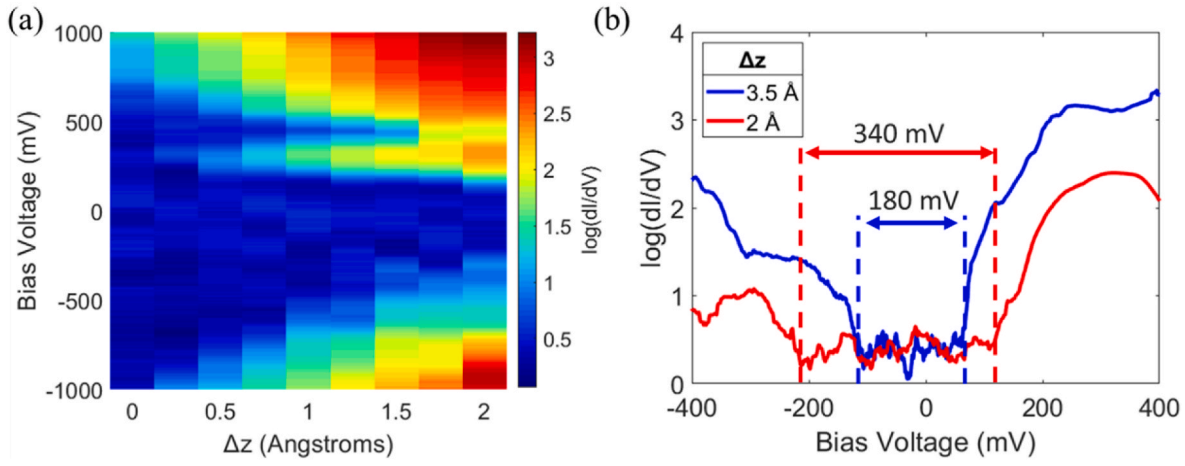

Fig. 3. Tip height dependent tunneling spectroscopy. (a) A color map of 9 tunneling spectra taken with varying tip-sample separation. The change in tip height $\Delta z = z_0 - z$ is used, where z_0 is the tip height at the set point conditions (+1.5 V, 0.053 nA). Positive Δz indicates the tip getting closer to the sample. The color scale represents the log of the dI/dV signal to enhance the contrast. (b) A direct comparison of the Δz = 2 Å spectrum from (a) and a spectrum taken with the tip as close as possible while maintaining stable tunneling Δz = 3.5 Å (+1.5 V, 0.025 nA). Data taken on Sample C.

[15,28]. This change in apparent band gap with varying tip-sample separation could be caused by an increase in the overlap between the tip and sample wavefunctions as the tip gets closer to the surface. The increase in wavefunction overlap leads to an increase in the measured d*I*/d*V* signal at lower bias voltages where there was not a detectable signal previously.

3.1.2. *Bi-terminated surface*

While the Se termination dominates the surface in most images (e.g., Figs. 1b), Fig. 4a shows an STM image of an area equally divided between Se and Bi terminations. In contrast to the Se termination, the Bi-terminated surface has a much higher density of bright, nanoscale protrusions on the surface, which we attribute to excess Se clusters left over from the removal of the Se capping layer in Sample A. Atomic resolution imaging of the Bi termination (inset in Fig. 4d) shows the expected triangular lattice with the same lattice constant as the Se termination. This indicates that the non-vdW surface does not reconstruct, which was also observed on the Bi termination of Bi_2Se_3 [29]. Additionally, dark triangular defects are not observed on the Bi termination which further differentiates it from the Se. There are a few point-like defects that could be attributed to the Mn_{Bi} antisite, however larger scale atomic resolution images that would allow us to compare with the antisite density of the Se termination were difficult to obtain.

We can also differentiate the Se and Bi terminations based on their electronic structure. Shown in Fig. 4b is a differential conductance (d*I*/d*V*) map taken at a bias voltage of −1.1 V where we find that two levels of contrast are revealed. Based on the corresponding topographic image we conclude that the bright and dark contrast areas correspond to the Se and Bi terminations, respectively. A similar dark contrast in dI/dV maps under these conditions was also associated with the smaller regions of Bi termination at the corners of peninsulas as in Fig. 1b, and also shown in Fig. S3. Similar differences in contrast were found between the Te and Bi terminations in d*I*/d*V* maps taken on Bi_2Te_3[19]. Additionally, STS was performed on both the Se and Bi terminations to help differentiate them based on their LDOS. Over the range in voltages where the Se-termination shows a gapped spectrum, the Bi-termination shows higher conductance with in-gap states (Fig. 4e). A similar spectrum of in-gap states were also observed on the non-vdW terminated surface of Bi_2Se_3, where the states were associated with the dangling bonds [29]. The presence of dangling bond states could explain the gapless nature of the Bi termination in our sample as well.

Interestingly, these large areas of Bi termination were only found on Sample A which had an amorphous Se capping layer that was removed prior to imaging. This is qualitatively similar to prior work on Bi_2Se_3, where Bi bilayer surfaces were obtained upon removal of Se by hydrogen adsorption [30]. In our studies, Samples B and C did show small areas of Bi termination at the corners of the SL peninsulas similar to Fig. 1c, but no large areas of Bi termination were observed. This suggests that the cap removal process can remove both the amorphous Se and Se associated with the vdW surface, but that small areas of Bi-termination can be found even in as-grown samples.

4. Conclusions

In summary, we have performed the first STM investigation on $MnBi_2Se_4$. We found that the surface is predominantly terminated in the Se layer adjacent to the vdW gap. The Se termination was found to have the expected hexagonal structure with the primary defect being Mn_{Bi} antisite defects in the subsurface Bi layer, which appear as dark triangular features on the Se termination with an abundance of about 10%.

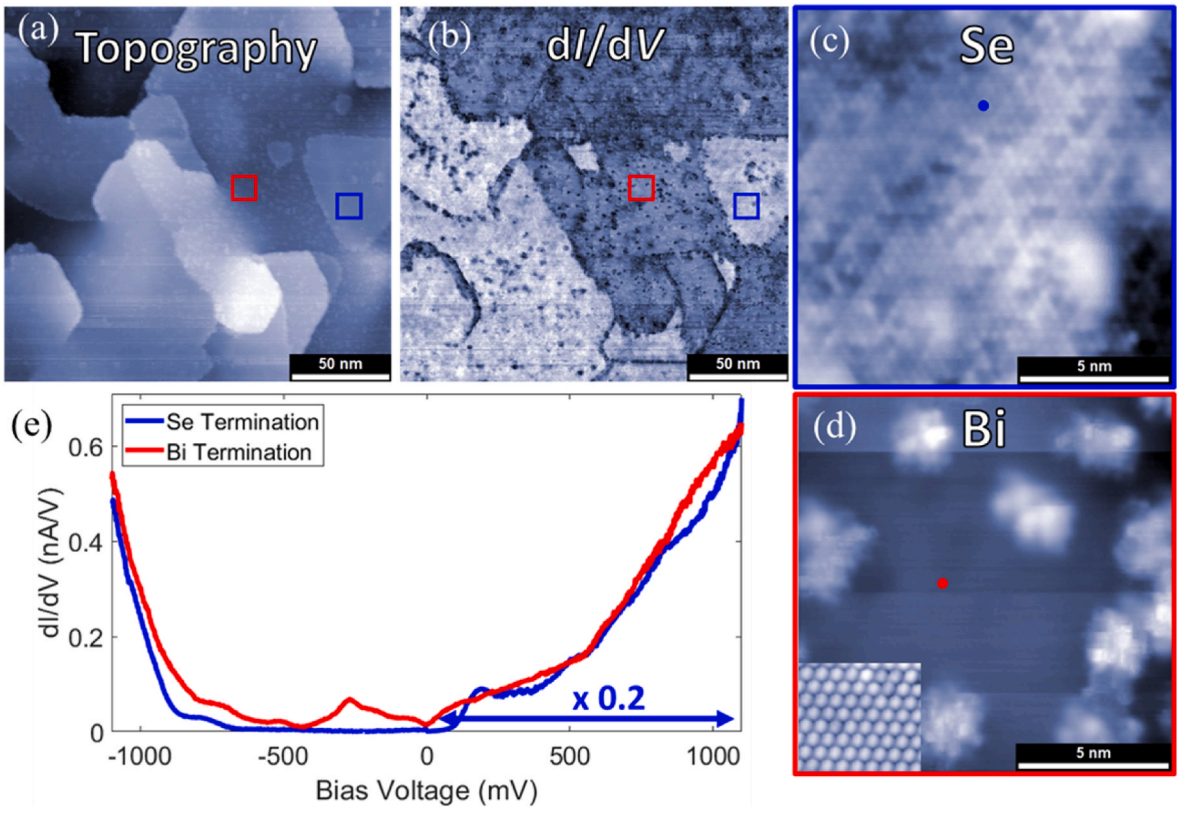

Fig. 4. Comparison of Se- and Bi-terminations. (a–b) Simultaneously acquired topographic (a) and dI/dV (b) images showing both the Se (light contrast in (b)) and Bi termination (dark contrast in (b)). Blue and red boxes represent the areas shown in (c) and (d), respectively. (c) Topographic image of the Se termination. (d) Topographic image of the Bi termination, with the inset showing an atomic resolution image of that termination. (e) Tunneling spectra taken on bare areas of the Se and Bi termination indicated by the dots in (c–d). The + V side of the Se termination spectrum is scaled by a factor of 0.2 for clarity. Data taken on Sample A (−1.1 V, 0.47 nA, V_{AC} = 50 mV_{rms}).

The Se termination was found to have a tip-height dependent apparent bandgap with a minimum observed value of 180 meV. Additionally, in the sample which had a Se capping layer applied and then removed, areas of Bi terminated surface were found that were on the order of 100 nm in size, whereas in samples with no cap only 1–10 nm patches of Bi termination were found. This work provides insight into the surface structure and electronic properties of a recently discovered and relatively unexplored A-type AFM topological insulator.

Author ccontributions

R.C.W. acquired and analyzed **STM** data and wrote the manuscript, **T.Z**. acquired **STM** data and grew samples, **A.J.B**. assisted in sample growth. All authors reviewed and contributed to the manuscript.

Declaration of competing interest

The authors declare that they have no known competing financial interests or personal relationships that could have appeared to influence the work reported in this paper.

Acknowledgements

We would like to thank J. J. Repicky and S. Shields for helpful discussions. This work was supported by the Department of Energy (DOE) Basic Energy Sciences under Grant No. DE-SC0016379.

Appendix A. Supplementary data

Supplementary data to this article can be found online at https://doi.org/10.1016/j.physe.2022.115391.

References

[1] R.S.K. Mong, A.M. Essin, J.E. Moore, Antiferromagnetic topological insulators, Phys. Rev. B 81 (2010), 245209.
[2] N. Varnava, D. Vanderbilt, Surfaces of axion insulators, Phys. Rev. B 98 (2018), 245117.
[3] J. Li, et al., Intrinsic magnetic topological insulators in van der Waals layered $MnBi_2Te_4$ -family materials, Sci. Adv. 5 (2019), eaaw5685.
[4] S. Chowdhury, K.F. Garrity, F. Tavazza, Prediction of Weyl semimetal and antiferromagnetic topological insulator phases in Bi_2MnSe_4, npj Comput Mater 5 (2019) 33.
[5] Y.S. Hor, et al., Development of ferromagnetism in the doped topological insulator $Bi_{2-x}Mn_xTe_3$, Phys. Rev. B 81 (2010), 195203.
[6] Y.L. Chen, et al., Massive Dirac fermion on the surface of a magnetically doped topological insulator, Science 329 (2010) 659–662.
[7] C.-Z. Chang, et al., Experimental observation of the quantum anomalous Hall effect in a magnetic topological insulator, Science 340 (2013) 167–170.
[8] M. Li, et al., Experimental verification of the Van Vleck nature of long-range ferromagnetic order in the vanadium-doped three-dimensional topological insulator Sb_2Te_3, Phys. Rev. Lett. 114 (2015), 146802.
[9] M.M. Otrokov, et al., Unique thickness-dependent properties of the van der Waals interlayer antiferromagnet $MnBi_2Te_4$ films, Phys. Rev. Lett. 122 (2019), 107202.
[10] H. Zhang, W. Yang, Y. Wang, X. Xu, Tunable topological states in layered magnetic materials of $MnSb_2Te_4$, $MnBi_2Se_4$, and $MnSb_2Se_4$, Phys. Rev. B 103 (2021), 094433.
[11] M.M. Otrokov, et al., Prediction and observation of an antiferromagnetic topological insulator, Nature 576 (2019) 416–422.
[12] Y. Gong, et al., Experimental realization of an intrinsic magnetic topological insulator, Chinese Physics Letters 36 (2019) 7.
[13] A. Zeugner, et al., Chemical aspects of the candidate antiferromagnetic topological insulator $MnBi_2Te_4$, Chem. Mater. 31 (2019) 2795–2806.
[14] C. Liu, Robust axion insulator and Chern insulator phases in a two-dimensional antiferromagnetic topological insulator, Nat. Mater. 19 (2020) 7.
[15] T. Zhu, et al., Synthesis, magnetic properties, and electronic structure of magnetic topological insulator $MnBi_2Se_4$, Nano Lett. 21 (2021) 5083–5090.
[16] S. Wimmer, et al., Mn-rich MnSb2Te4: a topological insulator with magnetic gap closing at high curie temperatures of 45–50 K, Adv. Mater. 33 (2021), 2102935.
[17] J.A. Hagmann, et al., Molecular beam epitaxy growth and structure of self-assembled Bi_2Se_3/Bi_2MnSe_4 multilayer heterostructures, New J. Phys. 19 (2017), 085002.
[18] S.V. Eremeev, M.M. Otrokov, E.V. Chulkov, Competing rhombohedral and monoclinic crystal structures in $MnPn_2Ch_4$ compounds: an ab-initio study, J. Alloys Compd. 709 (2017) 172–178.
[19] Urazhdin, S. et al. Surface effects in layered semiconductors $Bi_2Se_3$and Bi_2Te_3. Phys. Rev. B 7.
[20] J.-Q. Yan, et al., Crystal growth and magnetic structure of $MnBi_2Te_4$, Phys. Rev. Materials 3 (2019), 064202.
[21] Y. Yuan, et al., Electronic states and magnetic response of $MnBi_2Te_4$ by scanning tunneling microscopy and spectroscopy, Nano Lett. 20 (2020) 3271–3277.
[22] Z. Liang, et al., Mapping Dirac fermions in the intrinsic antiferromagnetic topological insulators $(MnBi_2Te_4)(Bi_2Te_3)_n$ (n = 0 , 1), Phys. Rev. B 102 (2020), 161115.
[23] Z. Huang, M.-H. Du, J. Yan, W. Wu, Native defects in antiferromagnetic topological insulator $MnBi_2Te_4$, Phys. Rev. Materials 4 (2020), 121202.
[24] F. Hou, et al., Te-Vacancy-Induced surface collapse and reconstruction in antiferromagnetic topological insulator $MnBi_2Te_4$, ACS Nano 14 (2020) 11262–11272.
[25] G. Lengel, Tunneling microscopy of point defects on GaAs(110), J. Vac. Sci. Technol. B 11 (1993) 1472.
[26] J.F. Zheng, et al., Scanning tunneling microscopy studies of Si donors (Si Ga) in GaAs, Phys. Rev. Lett. 72 (1994) 1490–1493.
[27] K.-J. Chao, A.R. Smith, C.-K. Shih, Direct determination of exact charge states of surface point defects using scanning tunneling microscopy: as vacancies on GaAs (110), Phys. Rev. B 53 (1996) 6935–6938.
[28] C. Nowka, et al., Chemical vapor transport and characterization of $MnBi_2Se_4$, J. Cryst. Growth 459 (2017) 81–86.
[29] H. Lin, et al., Topological dangling bonds with large spin splitting and enhanced spin polarization on the surfaces of Bi_2Se_3, Nano Lett. 13 (2013) 1915–1919.
[30] R. Shokri, et al., Atomic and electronic structure of bismuth-bilayer-terminated ${\text{Bi}}_{2}{\text{Se}}_{3}$(0001) prepared by atomic hydrogen etching, Phys. Rev. B 91 (2015), 205430.